Jamshidian and Rafe
Chem. Biol. Technol. Agric. (2024) 11:60
https://doi.org/10.1186/s40538-024-00579-9

Chemical and Biological Technologies in Agriculture

RESEARCH

Open Access

Complex coacervate of wheat germ protein/high methoxy pectin in encapsulation of D-limonene

Hamed Jamshidian[1] and Ali Rafe[1*]

Abstract

D-limonene is a volatile compound widely used in food flavorings, but it is chemically unstable in the presence of air, light, moisture, and high temperatures. Coacervation is a well-established technique which involves the formation of biopolymer nanocomplexes between negatively charged polysaccharides and positively charged proteins to protect bioactive components. The study shows the effect of pH, protein/polysaccharide ratio and total biopolymer concentration on complex coacervation of defatted wheat germ protein (DWGP) and apple pectin (high methoxyl pectin (HMP)) in the food industry as a carrier and delivery system for D-limonene. DWGP was used for the first time to form coacervate with apple pectin. Turbidity, ζ-potential and particle size of the complex coacervate and their individual biopolymers were examined for preliminary assays of complex coacervation. The optimum condition for DWGP/pectin complex coacervation was found to be at a ratio of 4:1 with a total biopolymer concentration of 1% and a pH of 4.0. The rheological properties of DWGP, pectin, and their coacervate were measured at various pH levels and ratios. The resulting coacervates, used to microencapsulate D-limonene, underwent spray-dried and were characterized using Fourier transform infrared spectroscopy (FTIR), scanning electron microscopy (SEM) and *X*-ray diffraction (XRD) measurements. These findings have the potential to contribute to the development of DWGP/pectin complex coacervates as effective delivery systems for volatile aromas or bioactive compounds.

Keywords D-limonene, Complex coacervation, Apple pectin, Wheat germ protein

*Correspondence:
Ali Rafe
a.rafe@rifst.ac.ir
Full list of author information is available at the end of the article

Graphical Abstract

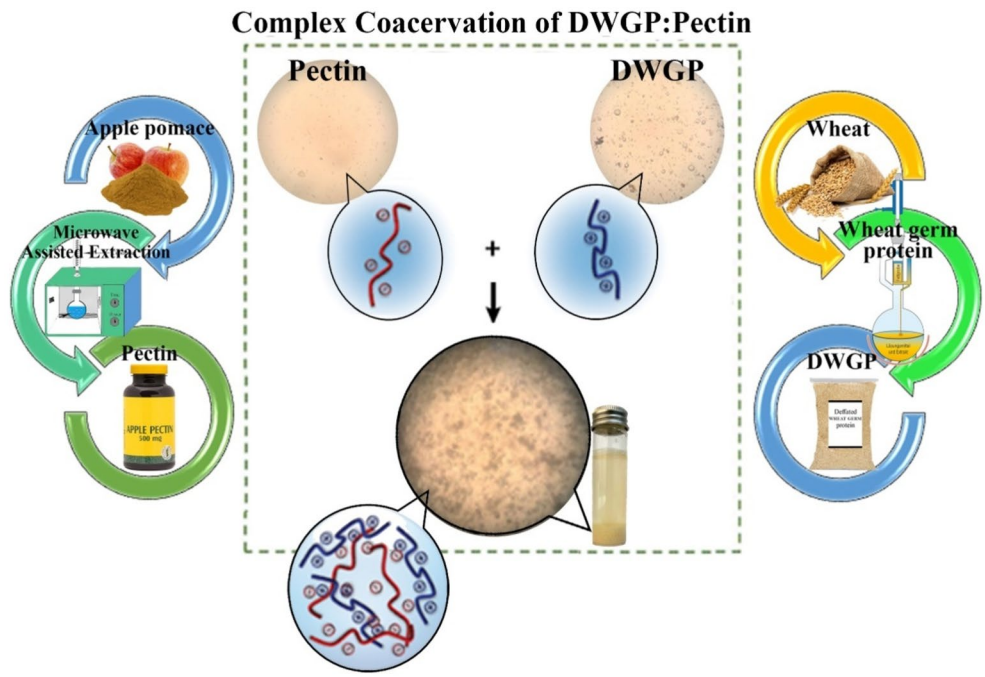

Introduction

D-Limonene ($C_{10}H_{16}$) is an important flavoring ingredient used widely in food products. D-Limonene is a clear liquid that belongs to the terpene family which are unsaturated hydrocarbons. This monoterpene can be found in the essential oils of lime, orange, dill, and cumin. It is a flavoring agent with antioxidant properties that can be dissolved in alcohol, but it is insoluble in water and barely soluble in glycerin. It is unstable under environmental factors such as light, air, and moisture. Therefore, extensive research has been conducted to identify techniques that protect this compound from damage during storage and production processes. Encapsulation is one of the most effective methods for maintaining the stability of sensitive substances, ensuring their targeted release within the product, and preventing undesirable interactions with food ingredients [1].

Defatted wheat germ (DWGP) contains about 30% protein (primarily albumin and globulin) [2, 3]. It is known that wheat germ protein contains the same amount of essential amino acids as animal proteins, including lysine, methionine, and threonine [3]. Therefore, wheat germ is a rich source of natural protein, especially in defatted form [4].

Pectin can be found in plants' cell walls, which has a polysaccharide structure. The main component of pectin is α-(1–4)-D-galacturonic acid, known as homogalacturonan (HG) [5, 6]. This structure also contains side branches with sugars such as rhamnose. Pectin is subdivided into low and high methoxy groups (< 50% and > 50%, respectively) [7]. The pectin structure makes it suitable for many applications in the food industry [8–11].

Complex coacervation, caused by electrostatic attraction between biopolymers including protein (Pr) and polysaccharide (Ps) with opposite charges (e.g., Pr–Ps, Ps–Pr, Pr–Pr), has been ultilized in developing encapsulation systems [1, 12–14], designing multilayer structures [15], controlling delivery systems [16, 17], as well as in food emulsions [8] and food structures [9, 10, 11, 18]. As the pH transitions from neutral to acidic, three critical pH values (pH_c, $pH_{\phi1}$, $pH_{\phi2}$) and four distinct regions can be distinguished (co-soluble complexes, soluble complexes, complex coacervates, and complex dissolutions). The highest turbidity was observed between $pH_{\phi1}$ and $pH_{\phi2}$, often referred to as the optimum pH (pH_{opt}), where the maximum amount of coacervates was produced [9, 19].

Several parameters can affect the structural properties of pectin, including biopolymer ratio, solvent properties, molecular mass, charge group density, pH, and ionic strength [20–23]. Coacervation and its functional attributes are influenced by the shape, composition, function,

molecular weight, and other properties of the biopolymer. Therefore, the type of biopolymer used in the coacervate process determines the final product attributes. Wheat germ protein is used in a wide variety of food applications due to its low cost, availability, high protein content, and essential amino acid composition.

In recent years, it has been found that protein and polysaccharide interact with each other to form electrostatic complexes that are influenced by parameters such as pH, ionic strength, mixing ratio, biopolymer concentrations and charge density [1, 16, 24–28]. To the best of our knowledge, the complex coacervation between DWGP and pectin has not been reported. Furthermore, the reaction between polymers may result in the formation of a new complex coacervate that can be used to preserve flavors, essential oils, and bioactive compounds in food products. Therefore, the present study is conducted to determine the effect of different pH levels, biopolymer ratios, and total biopolymer concentrations on the development of complex coacervation. The results provide insight into how DWGP and pectin form a complex and its use in the food industry.

Materials and methods

Material

The microwave extraction of pectin from apple pomace by mixing the dried apple pomace with HCl was performed according to the previous work [30]. After filtering, the extract was precipitated with ethanol 95% (v/v) in equal proportions. To remove mono- and disaccharides from the pectin mass, it was washed three times with ethanol 95% (v/v). It was then dried in an oven at 50 °C and kept in a desiccator. Dried pectin was stored in airtight bags (HDPE) in powder form.

DWGP was extracted by alkaline extraction and acid precipitation methods [31, 37]. Defatted DWGP suspension, was mixed with NaCl solution (0.5 N) for 30 min at room temperature, followed by centrifugation at 8582 g for 20 min at 4 °C. To precipitate the proteins, the supernatant solution was separated and the pH was adjusted to 4 with HCl (0.5 N) [32].

D-limonene and all other chemicals were analytical grade and were purchased from Sigma-Aldrich (St. Louis, USA).

Preparation of stock solutions

Apple pectin and DWGP (1% w/v) were dissolved in distilled water at ambient temperature and stirred for 2 h to prepare the stock solutions. Based on the pretreatment, initial concentrations were determined. An increase in turbidity and viscosity was observed at concentrations above 1%. To complete the hydration process, two solutions were placed in a refrigerator overnight [33].

Complex coacervation in D-Limonene encapsulation

According to our previous study, the optimal conditions for coacervation of DWGP and pectin were as follows: a mixing ratio of 4:1 w/w, Pr:Ps, with a total biopolymer concentration (C_T) of 1% w/v (Jamshidian et al., 2022). Therefore, mixtures of DWGP and pectin were prepared at R = 4:1 with C_T = 1% at 25 °C and pH 7.0. The solutions were then placed in an ice-water bath to gradually lower the temperature below 10 °C under constant stirring to promote complex coacervation. Afterwards, Tween 80 (10% of the total solids) was then added and stirred until completely dissolved [36]. Finally, D-limonene was gradually added to this solution at pH = 4 under ultrasonic homogenization (Iranian Ultrasonic Company, 400 W, 20 kHz, 12 mm probe diameter) at ambient temperature and 350 W for 10 min [1]. Then, the capsules were dried using a spray dryer (spray drying process creates capsules with high sphericity, which allows them to retain more compounds). The samples were spray-dried using B-191 mini spray-dryer (BÜCHI Labortechnik AG, Flawil, Switzerland) at 180 ± 10 °C inlet temperature, 80 ± 10 °C outlet temperature, 10.0 mL/min feed rate, 4 bar compressed air pressure, and 0.60 m^3/h air flow rate.

Complex coacervation characteristics measuremnets

A UV–vis spectrophotometer (Jenway, 6305, London, England) calibrated to 100% transmittance (T%) with ultrapure water was used to determine the pH-dependent turbidity at a wavelength of 600 nm. Turbidity was determined by absorbance (%ABS) and the pH of the solution was adjusted with 1, 0.1, and 0.01 N HCl at room temperature (pH meter; Metrohm, 744, Herisau, Switzerland). The turbidity of the solution increased during acidification, and the pH_c, $pH_{\phi 1}$ and $pH_{\phi 2}$ are shown graphically [34]. It has been observed that turbidity and reaction between two polymers are most prominent at pH_{max} [33, 35]. The zeta potential was measured in the

Table 1 Chemical features of DWGP and apple pectin

Parameters	DWGP	Apple pectin
Moisture (w_b)	9.88 ± 0.26	8.10 ± 0.11
Methoxy groups	–	9.02 ± 0.01
Galacturonic acid	–	68.53 ± 0.57
Degree of esterification	–	75.00 ± 0.10
Eq.W	–	929.01 ± 2.05
Ash	4.68 ± 0.22	–
Fat	0.75 ± 0.42	–
Protein (N × 5.7)	75.63 ± 0.26	–
Carbohydrate	9.07	–

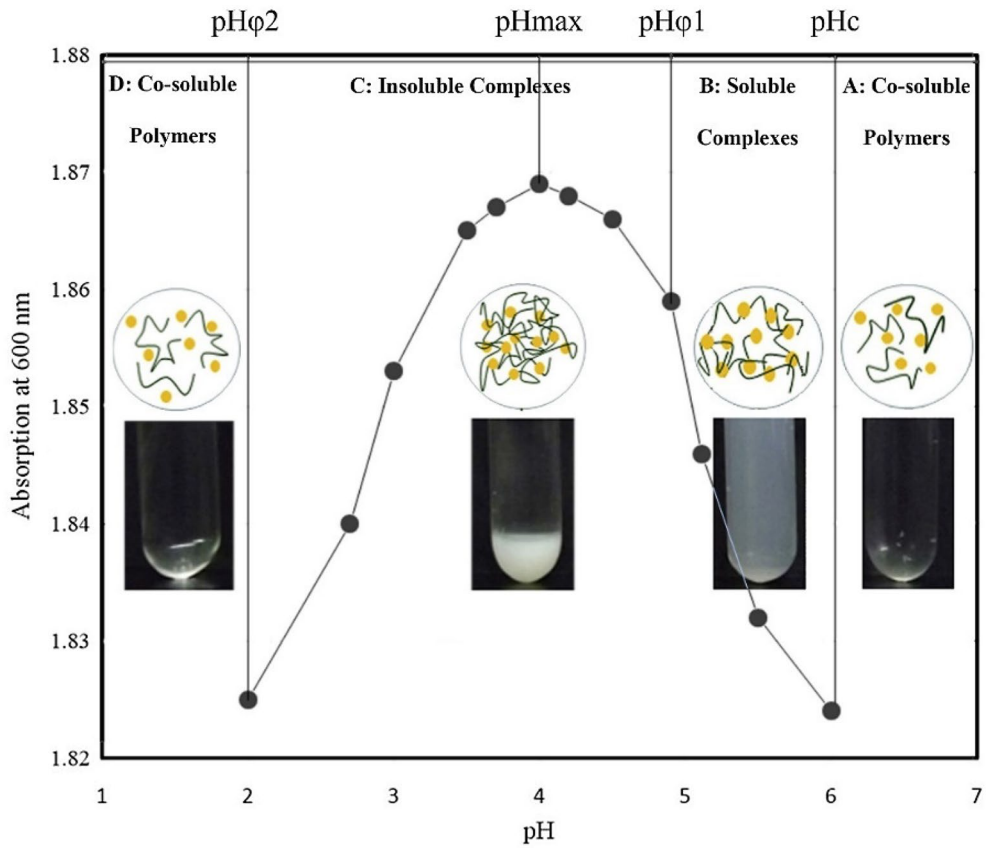

Fig. 1 Turbidity curve of DWGP–pectin mixture during acidification (in $R = 4{:}1$ and $C_T = 1\%$) and the 4 sections and pH divisions

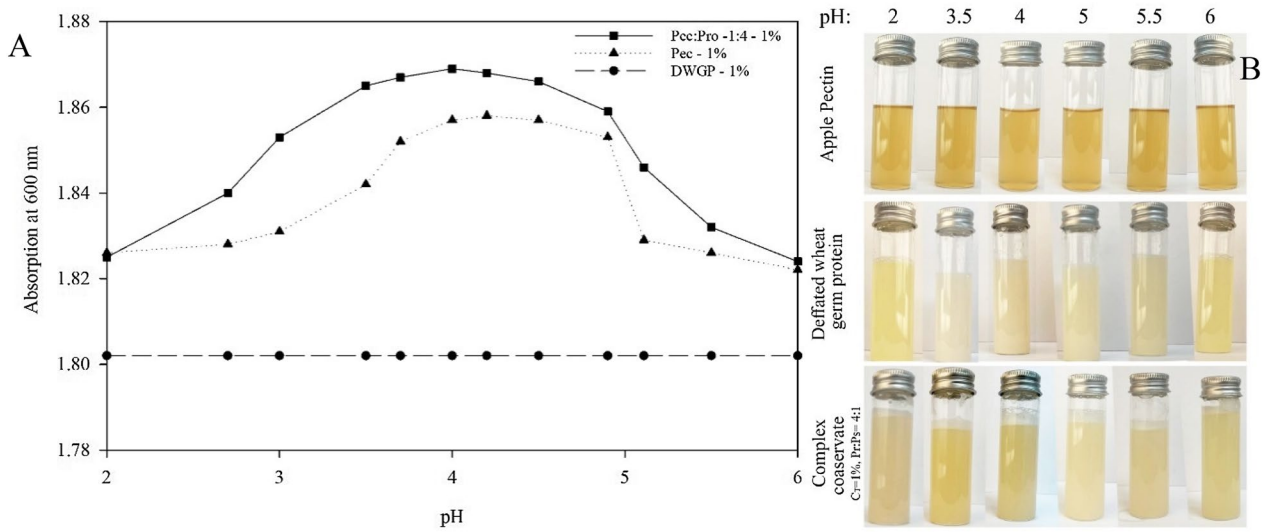

Fig. 2 Evolution of absorbance as a function of pH for DWGP, pectin at 1% and mixture of DWGP–pectin ($C_T = 1\%$ and $R = 4{:}1$) numerically (**A**) and visually (**B**)

range of pH 2 to 5.5. Z-potentials were determined using a dynamic light scattering (DLS) instrument (HORIBA, SZ-100, Minami-ku Kyoto, Japan). The diffusion coefficients (D, m^2/s) as a function of pH were measured to determine the hydrodynamic diameters of the complexes (R=4:1, C_T=1%) and their constituent biopolymer solutions. The solutions were placed in the He–Ne laser path with a wavelength of 633 nm for dynamic light scattering (DLS) measurement at different pH levels (HORIBA, SZ-100, Minami-ku Kyoto, Japan) [35, 36].

Rheological Measurements

A Brookfield viscometer (Viscolead one L., Fungilab, spindle S00, Spain) was used to determine the viscosity of the samples (16 ml) under a shear rate of 18 to 170 s^{-1} at ambient temperature.

Characterization

Structural properties using FTIR

The DWGP, pectin, and DWGP/ pectin coacervates were characterized by FTIR spectroscopy (a double-beam spectrometer, Bruker FTIR-Tensor 27, Ettlingen, Germany) with 64 scans at 4 cm^{-1} resolution over the wavelength range from 4000 to 400 cm^{-1} (mid-infrared region) using the KBr pellet method. The infrared spectrum of pure KBr was selected as the baseline[3].

Morphological characterization (SEM)

The morphological properties of the microcapsules were assessed using a scanning electron microscopy (SEM; Philips, Philips XI30, Netherlands). DWGP, pectin, DWGP/pectin coacervates, D-limonene, and DWGP/ pectin coacervates with D-limonene were mounted onto an amorphous glass lamella and coated with a thin layer of gold prior to taking images. At least three images of typical structures were acquired at 60 and 250 magnifications using an accelerated voltage of 20 kV.

X-ray diffraction analysis (XRD)

The XRD patterns of DWGP and pectin powders and their coacervates were determined with an X-ray diffractometer (PMD Philips X-Pert, Philips Company, Netherlands) at 25 °C. The instrument was operated under Cu-K-alpha^{-1} radiation, a target voltage of 45 kV, a current of 30 mA, and a diffraction angle range of 10–100° (2θ) with a scan rate of 0.02/sec.

Sodium dodecyl sulphate–polyacrylamide gel electrophoresis (SDS-PAGE)

SDS-PAGE was performed according to a modified method described by Laemmli (1970) under reducing conditions [29]. A 5% stacking gel and a 12.5% separating gel containing 0.4% SDS were used. Samples were prepared by dissolving 2 mg/ml (DWGP) or 4 mg/ml (other) sample powder in demineralized water. 60 µl of each solution were mixed with 20 µl of the ready-to-use buffer Roti Load 1 (Carl Roth, Karlsruhe, Germany). Then, aliquots (20 µl) were loaded onto the gels. The gels were run in a Tris-Glycin running buffer containing 0.1% SDS at 90 V (20 mA). Electrophoresis was stopped when samples reached the bottom of the gels (after 1.5–2 h). Proteins were stained by Coomassie Brilliant Blue R250 in 10% acetic acid. For destaining, a solution of 10% acetic acid and 25% methanol was used. To estimate the molecular weight of samples, the protein standard Precision Plus Protein™ Dual Color (Bio-Rad Laboratories Inc., Hercules, CA, USA) containing weight markers from 10–250 kDa was used [29].

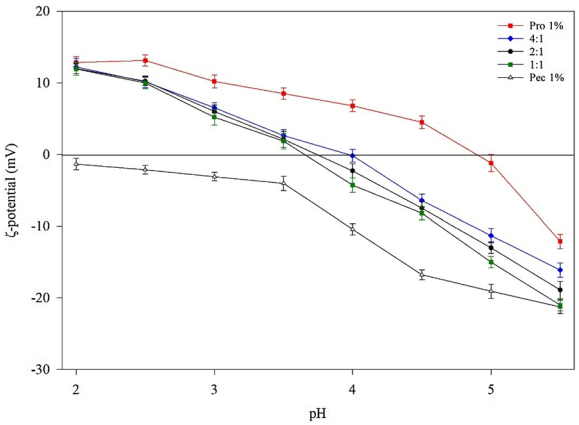

Fig. 3 ζ-potential (mV) of DWGP and pectin (1%, w/v), and mixture there of (C_T= 1%, w/v) with different R (1:1, 2:1 and 4:1 w/w)

Statistical analysis

Experiments were performed in at least three replicates. Data were analyzed by a one-way analysis of variance (ANOVA) with a significance level of 95% ($P<0.05$). All data were analyzed using SPSS and GraphPad Prism.

Results and discussion

Physicochemical properties

The composition of the biopolymers (DWGP and apple pectin) are shown in Table 1.

Effect of pH on the DWGP-pectin interactions

The pH of the solution plays a critical role in the formation of coacervates by adjusting the electrical charges on the surface of polymers. Phase changes occur mainly between pI (protein) and pKa (pectin) [36]. The turbidity curve of biopolymers and their complexes as a function

Table 2 Particle size of DWGP and pectin (1%) and DWGP–pectin mixture (Pr:Ps 4:1) at different pH values

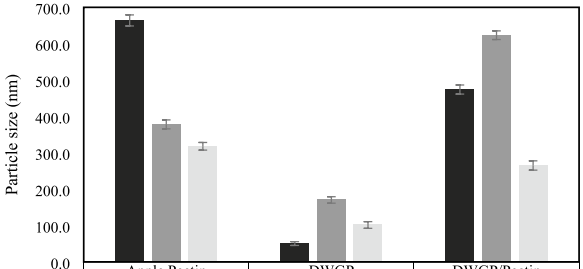

	Apple Pectin	DWGP	DWGP/Pectin
pH=5.5	664.0	50.7	474.1
pH=4	378.3	170.5	623.4
pH=2.5	318.1	101.7	265.3

of pH (2.0–6.0) is shown in Fig. 1. Following the reduction of the pH of the solutions during the measurement of turbidity, four sections (A, B, C, and D) as well as four critical pHs (pH_c, $pH_{\phi1}$, pH_{opt} and $pH_{\phi2}$) were identified. Part A (co-soluble section) shows that the turbidity of the solutions remains constant above pH_c (6.0). Part B (soluble complex section) indicates that the turbidity of DWGP-pectin mixtures rose slightly as the pH decreased to $pH_{\phi1}$ (4.9) [25]. As acidification increased, the turbidity increased considerably and insoluble complexes were formed below $pH_{\phi1}$, likely due to the formation of insoluble coacervates of protein and pectin. A maximum turbidity is achieved at pH_{opt} (=4). The electrical charges of the system have been neutralized at pH = 4.85 (ζ-potential = 0), confirming the value of pH_{opt} (C: insoluble complex region). Protein-polysaccharide interactions are generally weakened when the net negative charge of the complexes is reduced [37, 38]. Similar findings have been also reported by Ach et al. (2015) and Souza and Garcia-Rojas (2017) [39, 40].

The turbidimetric titration curves (pH 2.0–6.0) and the appearance of DWGP (0.06%), pectin (0.04%) and their mixture (R = 4:1) at C_T = 1% are presented in Fig. 2.A and B. The pectin solution was clear at all pH levels, regardless of the pH level, while the DWGP solution was cloudy at all pH levels. Turbidity was increased by decreasing the pH of the DWGP solution. The highest turbidity was observed at pH = 4.2, while the turbidity decreased as pH rose, indicating that the solubility of wheat germ protein is pH-dependent [36]. Turbidity increases as the number and size of particles increase [41]. The mixed solution with R = 4:1 at C_T = 1% is actually divided into two phases, the deposition of protein particles and the clear upper phase [42, 43].

The turbidity of the pectin was lower than that of the complex during acidification. This slight change during acidification is attributed to the polysaccharide structure [34]. Defatted wheat germ protein and apple pectin were negatively charged at pH_c = 6.0. The negative charge and electrostatic repulsion of the negative charges on DWGP and pectin at pH_c = 6, prevents coacervate formation [44]. Similar reports have been published by Liu et al. (2015 & 2017) [45, 46]. The DWGP-pectin mixture was also stable at pH 5.1 to 5.5, indicating that no phase separation occurred. The turbidity of the mixture (R = 4:1, CT = 1%) reached its maximum value (1.869) at pH = 4 (pH_{max}), which indicates the high amount of insoluble complexes and electrostatic bonding. Further decrease of pH below 4 resulted in a noticeable decrease of turbidity, due to protonation of pectin carboxyl groups and destruction of complexes. At pH 2.0 ($pH_{\phi2}$), separation of the complexes occurs due to the equal charge of the biopolymers [34].

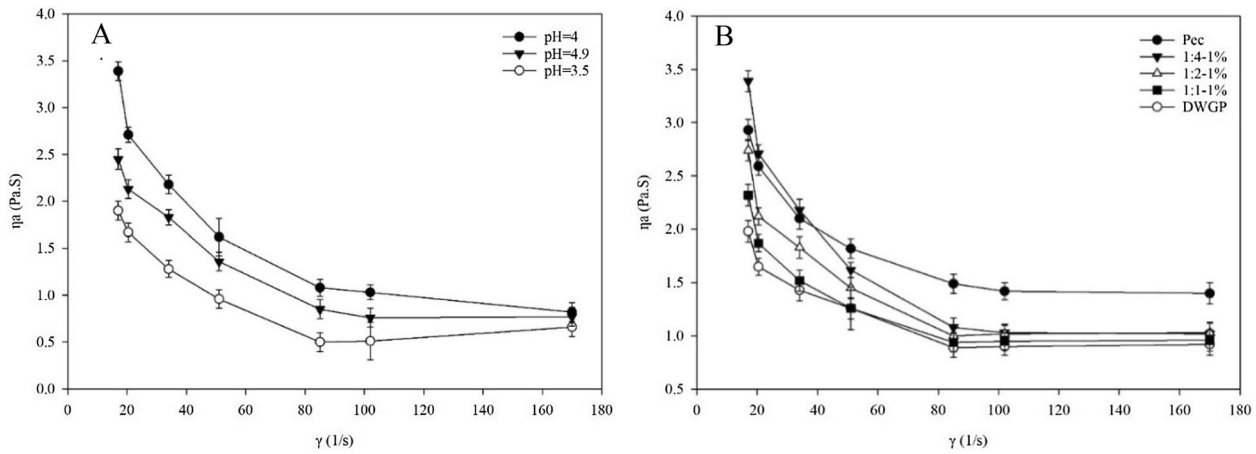

Fig. 4 Flow curve of DWGP/apple pectin coacervates (C_T = 1%—Pr:Ps = 4:1) between apparent viscosities and shear rate (**A**) and different ratios of protein to pectin at optimal pH (=4) (**B**)

Interactions between whey protein isolate and flaxseed gum also yielded in similar results [46].

ξ-potential

The ζ-potential of homogeneous solutions of DWGP, pectin, and their mixtures, was monitored at different ratios (4:1, 2:1, and 1:1 w/w) and pH values (2.0–5.5) (Fig. 3). The surface charge of the protein ranges from a negative value (− 12.1 mv) at pH 5.5 to a positive value (12.87 mv) at pH 2, with a zero load point (IP) around 4.85. The zeta potential of proteins is pHdependent due to their amphoteric properties (containing both amino (NH_2) and carboxyl (–COOH) groups simultaneously). In addition, the ζ-potential of the protein decreases with increasing pH. The decrease in ζ-potential can be attributed to the change of charges in carboxyl and amino groups with increasing pH. Furthermore, pectin is an anionic polysaccharide with a negative charge [45]. Pectin molecules are less likely to undergo carboxylate ionization as pH decreases [47]. As can be seen, the mixture of biopolymers has average values of the individual solutions.

The zeta potential increased as R increased from 1:1 to 4:1 (Fig. 3), probably due to the higher ζ-potential of protein than pectin. When R is increased from 1:1 to 4:1, the IP increases from 3.65 to 3.93. The highest turbidity was observed near pH 4.0 in the 4:1 ratio mixture [40], confirming the electrostatic interaction between the carboxyl groups of pectin (− 10 mV) and the amine groups of protein (±5 mV) [48]. Thus, electrostatic reactions are the primary cause of coacervate formation. Pectin and protein form the most stable bond at pH_{max} [19, 49]. The FTIR results of protein-pectin coacervates have also demonstrated that intermolecular reactions are responsible for the formation of coacervates [36].

Particle size

To gain a deeper understanding of the interaction between DWGP and pectin, the particle size distribution of the two biopolymers was analyzed using DLS during the preparation of complex coacervates [43]. This parameter is used to investigate the formation and deveolopment of protein-polysaccharide complexes. As shown in Table 2, the particle size of homogeneous solutions of DWGP and pectin (1%), as well as their 4:1 mixture ($C_T = 1\%$), was measured at three pH levels (5.5, 4.0, and 2.5). As pH decreased from 5.5 (50.70 nM) to 4.0 (170.53 nM), larger aggregates were formed. Protein size is increased at pH 4.0 due to the repulsion reduction and the accumulation of DWGP [50]. As acidification increases, it increases the positive and identical charges, which improves the solubility of proteins.As acidification increases, it increases the positive and identical charges, which improves the solubility of proteins. This in turn results in increased solubility and a decrease in large and insoluble particles. Meanwhile, pectin particle size remained constant as acidification progressed [16].

The complex size was 474.27 mm at pH 5.5, which was smaller than that of pectin. The particle size of pectin has a profound effect on the size of soluble complex particles. It has been demonstrated that the contraction of molecules can reduce the size of complex particles. In the range of soluble complexes (pH ~ 5.5), there is no correlation between particle size and turbidity, and this is caused by the increase in molecular weight of the compounds. Therefore, the results of this section are slightly different from those of the turbidity measurement section. The particle size increased to 474.27 nm at pH 5.5. This is consistent with the results reported in the insoluble complexes formation section. The formation of insoluble complexes reached its maximum level at pH 4 where the maximum diameter of the particles (623.37 nm) was

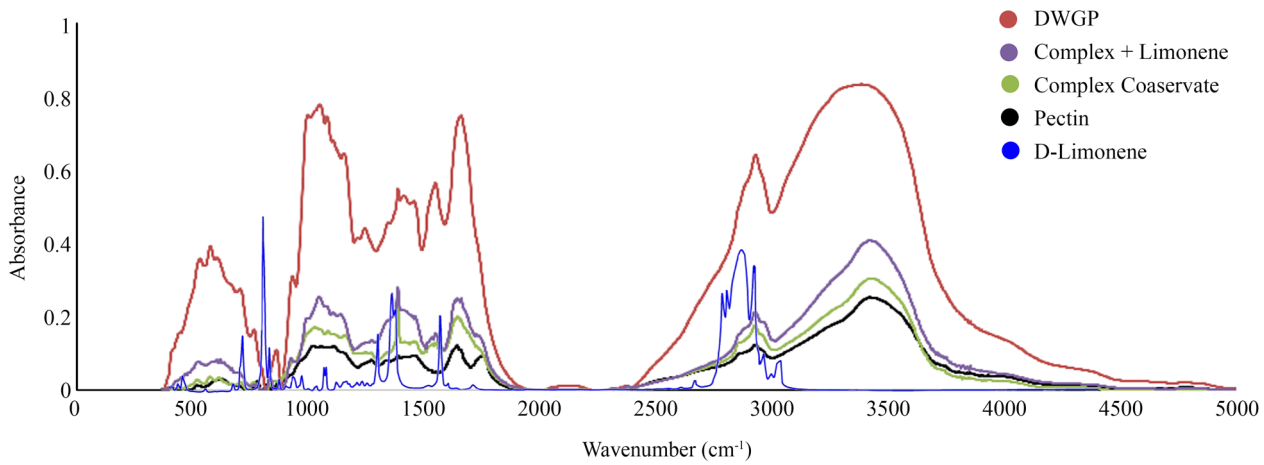

Fig. 5 FTIR spectra of DWGP, pectin, DWGP/pectin coacervates, D-limonene and DWGP/pectin coacervates with D-limonene

also detected (Table 2). The insoluble complexes are possibly to be decomposed and separated at acidic pH values due to the seperation of pectin carboxyl groups.

Rheological properties

Viscosity is the ratio of shear stress to shear rate that describes the substance's resistance to flow. Viscosity is determined by the concentration of biopolymers, their interaction with solvents, as well as their structural properties, including their size, shape, and flexibility.

The viscosity of polysaccharide solutions is higher than that of protein solutions. Figure 4 illustrates the viscosity characterization of pectin and DWGP solution (1%), along with their complex coacervation at $C_T = 1\%$ and Pr:Ps, 4:1. As can be seen, pectin exhibits non-Newtonian behavior characterized by a decrease in dynamic viscosity as a function of increasing applied shear stress under a shear stress less than 50 s^{-1}. The shear-thinning behavior of pectin is attributed to the weakening of the intermolecular forces between its molecules with increasing shear rates [51, 52]. In fact, the apparent viscosity of the pectin solution decreased rapidly with increasing shear rates, from 15 to about 50 s^{-1}, but remained almost constant at very high shear rates. At low shear rates (less than 50 s^{-1}), a shear thinning non-Newtonian behavior is observed, while at higher shear rates, approximately between 50 and 170 s^{-1}, Newtonian behavior is detected [52]. DWGP exhibits non-Newtonian and time-independent behavior. The effects of pH on coacervates was examined at three pH levels: the pH at the onset of coacervate formation (4.9), the pH optimal for coacervate formation (4), and the pH at the beginning of coacervate degradation (3.5). To investigate the effect of the proteintopolysaccharide ratio on flow behavior, coacervates with ratios of 1:1, 2:1, and 4:1 were used at optimal pH (Fig. 4-B). Complex coaservates showed a shear-thinning behavior at different pH levels (Fig. 4-A). The shear thinning behavior is caused by the breaking or reconstruction of the structure of the coacervates when it is subjected to shear force [36, 53]. The coacervate has a higher viscosity at pH = 4 than other pHs, indicating a denser structure caused by electrostatic interactions between protein and pectin molecules [36, 54]. The viscosity of coacervates appears to be directly related to the strength of electrostatic bonds in polyelectrolytes. When the pH is higher or lower than the optimal pH, coacervate exhibits a less dense structure, resulting in lower apparent viscosity, which is highly pH dependent [36]. Similar findings have been reported for chitosan-arabic gum coacervate [47], sodium caseinate-tragacanth gum [55], carboxymethyl cellulose-arabic gum [56], whey protein-linseed gum [46], and whey protein-high methoxy pectin [57].

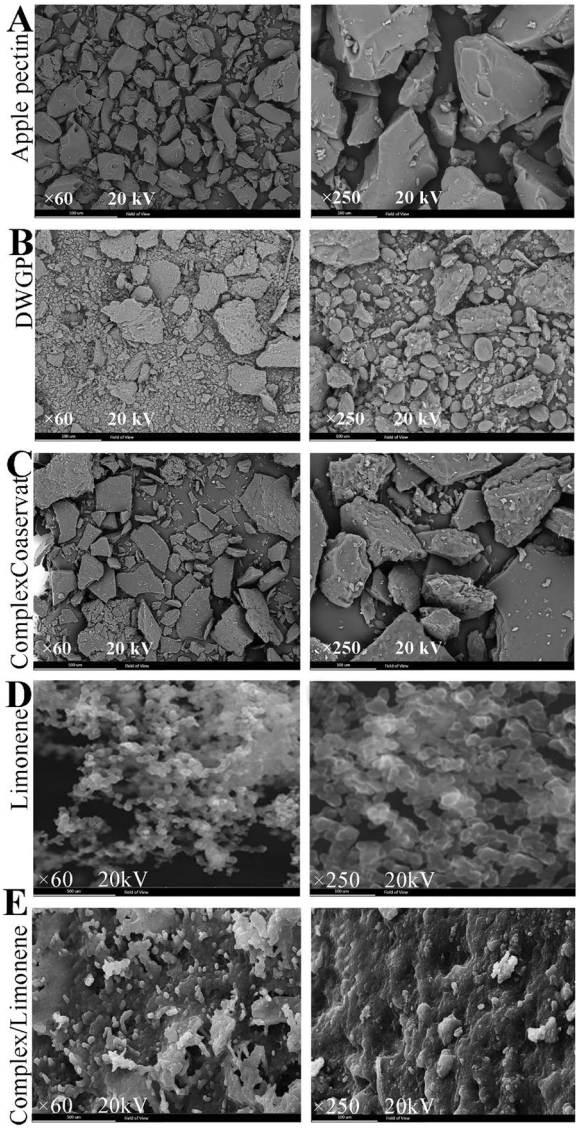

Fig. 6 SEM micrographs of the apple pectin (**A**), DWGP (**B**), DWGP/pectin coacervates (**C**), D-limonene (**D**) and DWGP/pectin coacervates with D-limonene (**E**) at 60 and 250 × magnification, 20 kV

FTIR analysis

The infrared spectra of DWGP, apple pectin, complex coacervate and complex coacervate with D-limonene are shown in Fig. 5. The FTIR spectroscopy of proteins provides useful information about their secondary structure. The secondary structure of proteins is primarily determined by their amide I region, which exhibits the stretching vibration of carboxyl groups [58]. The FTIR spectrum of DWGP exhibits a strong band at1666 cm^{-1} corresponding to the vibrational state of the 1st type of amide, characterized mainly by C = O stretching vibrations and partially by N–H peptide bonds. In addition, the peak

observed at 1554 cm^{-1} is associated with the second type of amide structure (N–H and C–N stretching shape changes) and the peak at 1273 cm^{-1} corresponds to the third type of amide structure (N–H and C–N stretching shape changes) [59].

It is believed that the peaks in the wave number of 1450 and 1416 cm^{-1} reflect vibrations in the CH_2 and CH_3 groups. Aliphatic amino acids and proteins show C–H stretching vibrations in the range of 2850–3320 cm^{-1} [60]. Apple pectin presented broad peaks at wave numbers of 3388 and 2941 cm^{-1}, which represent negatively charged carboxylic groups (O–H stretching bands and C–H vibrational bands, respectively). Furthermore, in accordance with other researchers, the peak at 1749 cm^{-1} was attributed to the methyl ester ($COOCH_3$) and undissociated carboxylic acid (COOH) groups [61]. Based on previous studies, the peaks at 1630 cm^{-1} are caused by the asymmetric stretching vibration of the carbonyl group of the carboxylate ion (–COO) and the amide I structure (C = O and C–N stretching) [62, 63]. It is thought that the absorption bands around 1300 and 1450 cm^{-1} are related to the asymmetric stretching vibrations of the carboxylic group, while the band at 1020 cm^{-1} is related to the main chain of the polysaccharide structure (C–O–C)[64, 65].

The spectrum of complex coacervate shows almost equal peaks for both biopolymers, but due to the higher protein-to-pectin ratio (1:4), the spectrum of the complex is more similar to that of pectin. The weaker and broader –OH stretching vibration at wave number 3000–3500 cm^{-1} indicates that a limited hydrogen interaction occurred between pectin and protein during coacervate formation. There are significant differences in the amine and carboxyl regions of the coacervate spectrum compared to protein and pectin, which indicates electrostatic interactions between them. It is consistent with the results of Sun et al. [66] for complex coaservate of propylene glycol alginate. According to Gilsenan et al. [67], hydrogen bonding contributes significantly to the formation of pectin-gelatin coaservates. Moreover, Guerrero et al. [68] demonstrate the formation of hydrogen bonds in soy protein isolate-agar coacervate. The spectra of DWGP and apple pectin coacervate exhibit two peaks at 1657 and 1548 cm^{-1}, which are caused by stretching vibrations of –COO– and NH^{3+} groups. The peaks associated with the first, second, and third amide types shift from 1666, 1554, and 1273 cm^{-1} in protein to 1657, 1548, and 1270 cm^{-1} in coacervate, respectively, and their intensities decrease significantly. The electrostatic interactions between the apple pectin negative charge and the DWGP positive charge may account for these changes. In general, hydrogen bonds and electrostatic interactions play a major role in the formation of complex coacervates of DWGP and apple pectin.

In D-limonene, there are three broad peaks associated with the C–H stretching band at wave numbers 2967, 2922, and 2837 cm^{-1}, while the C–O stretching band is associated with the peak at wave number 1642 cm^{-1}. A strong peak at 886 cm^{-1} suggests a change in the C–H bond of the ether group, whereas the peak at 798 cm^{-1} reveals a bending of the C–H bond of the phenol group [69–71]. Coasarvate has a peak at wave numbers of 1657 cm^{-1} and 1548 cm^{-1} associated with stretching vibrations of the –COO– and NH^{3+} groups, respectively, as well as peaks corresponding to the 1st, 2nd, and 3rd types of amides at wave numbers of 1657, 1548, and 1270, respectively. The spectrum of the capsule does not reveal any D-Limonene indicator peaks (wave numbers 886 and 798 cm^{-1}), which indicates that microencapsulation of D-Limonene was successful. Several studies have addressed this issue previously [72, 73].

Morphological properties (SEM)

An electron microscope image of pectin, DWGP, complex coacervate dried with a spray dryer, D-Limonene, and complex coacervate containing D-Limonene is presented in Fig. 6. DWGP has a spherical appearance characterized by a rough and cluster-shaped surface. A polar group is believed to be responsible for the roughness of the surface of globular proteins. Furthermore, it is arranged in clusters with dense three-dimensional networks, similar to milk proteins images at the isoelectric point. The surface of apple pectin is characterized by irregular polygons with grooves. The morphology of pectin powder showed a large number of columns/sheets interspersed with small fragments. In the SEM micrograph of the complex coacervate, a non-porous, non-uniform layer is evident with aggregation while limonene was encapsulated (Fig. 6. E). When the particles are being dried, water rapidly evaporates from their surfaces, resulting in wrinkles on their surfaces. As compared to pectin and protein, coacervate has a networked and porous structure, which indicates electrostatic interactions between pectin and protein. Coacervates contain vesicles of different sizes on their surface, which have the potential to trap sensitive compounds [63].

According to the XRD diagram (Fig. 7), D-limonene has an amorphous structure. Coaservates containing D-limonene are less amorphous (semi-crystalline) than pure D-limonene. As mentioned earlier, the DWGP/apple pectin complex coacervate is composed of a non-porous and non-uniform layer. The absence of cracks or porosity on the surface of the particles indicates that the wall material has to some extend covered the core material, demonstrating the success of the coating process. A major contributing factor to this problem is the use of the spray drying method [63].

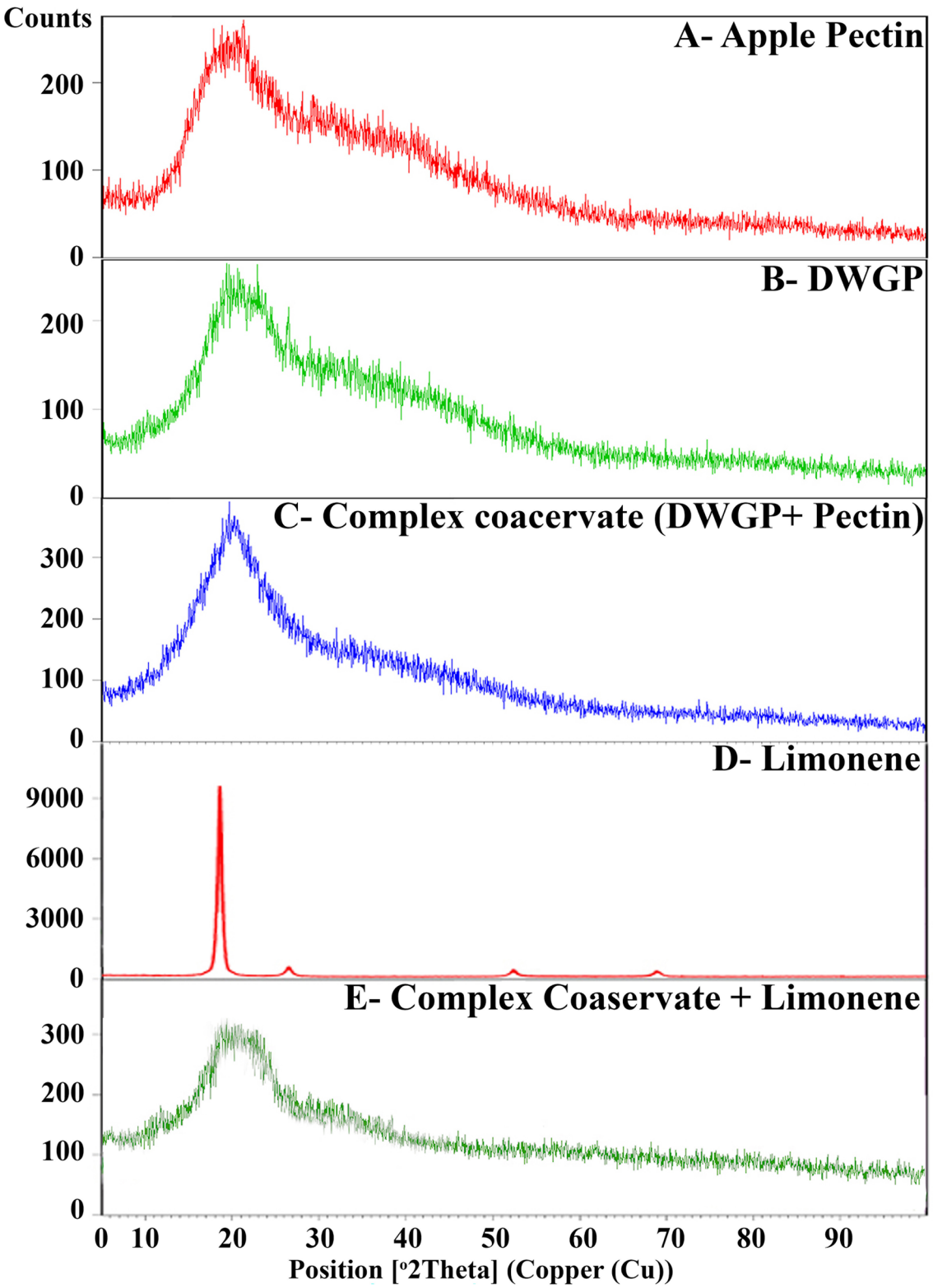

Fig. 7 X-ray diffraction comparison of pectin (**A**), DWGP (**B**), their complex coacervate (**C**), D-limonene (**E**) and complex coacervate with D-limonene

X-ray diffraction analysis (XRD)

X-ray diffraction is used to determine the degree of crystallinity and the type of structure of materials. A spectrum with sharp peaks indicates crystalline character, whereas a spectrum with broad peaks indicates an amorphous structure. X-ray diffraction patterns of apple pectin, DWGP, complex coacervates of DWGP/pectin, D-Limonene and complex coacervates of DWGP/pectin with D-Limonene are shown in Fig. 7.

There are four sharp peaks found in DWGP, at 19.5, 22, 26.5 and 29 degrees (2Θ) (Fig. 7B), which indicates its crystal structure. *X*-ray difraction patterns of the protein showed two peaks at 10 and 22°, indicating the presence of α-helix and β-sheet structures, respectively. A lack of a peak in the x-ray pattern of DWGP at 10° confirms the FTIR results and the fact that DWGP's structure contains more β-sheet than α-helix. It was found that pectin has amorphous structure along with semi-crystalline structures in 21 and 28° (2Θ), respectively, which indicates lack of molecular order [74].

The *X*-ray diffraction pattern of complex coacervate shows a peak at 20° (Fig. 7C), which indicates its amorphous structure. The disappearance of protein and pectin peaks in coacervate indicates that electrostatic interactions and hydrogen bonds have formed between pectin and protein, leading to changes in its crystal structure, as confirmed by FTIR. The structure of the complex coacervate of DWGP/apple pectin is generally amorphous.

According to *X*-ray diffraction analysis of the complex, the sharp peak of D-limonene (20°) was eliminated, suggesting that D-limonene was fully incorporated. Furthermore, the removal of protein and pectin peaks in coacervate suggests that electrostatic interactions and hydrogen bonds have been formed between pectin and protein, resulting in changes in its crystal structure. In general, DWGP/pectin complex coacervates have an amorphous structure. The XRD patterns of the loaded samples revealed only one concentrated peak at 22°, indicating that the capsules had become amorphous following the addition of D-limonene (Fig. 7E). As a result of these structural changes in the amorphous capsule matrix, molecular mobility increases, resulting in a decrease in encapsulated compound retention.

Table 3 Distribution and protein content of protein fractions of DWGP[a] [65]

	% of total protein[b]	Protein content %[c] (db)
Albumin	34.5 ± 1.10a	33.4 ± 0.60c
Globulin	15.6 ± 0.53b	82.7 ± 1.51a
Prolamine	4.6 ± 0.20d	11.6 ± 0.85d
Glutelin	10.6 ± 0.20c	75.6 ± 1.22b
Insoluble residuesd	34.7	–

[a] Values are mean ± standard deviation of three replicates. Means followed by the same letter in the same column are not significantly different ($P < 0.05$)

[b] % of total protein = [total proteins (*g*) of each fraction extracted from 100 g of meal/total proteins (*g*) of 100 g of defatted wheat germ meal] × 100

[c] Protein content % = g of proteins in 100 g of extracted solids

[d] Insoluble residues = 100–(albumins + globulins + prolamins + glutelins)

SDS-PAGE

Protein fractionation was performed according to the classical method of Osborne (1924) with minor modifications [65]. The distribution and protein content of protein fractions in DWGF are presented in Table 3. The globulin fraction had the highest protein content followed by glutelin, albumin, and prolamine. A large amount of carbohydrates and pigments were extracted into the albumin and prolamine fractions causing their low protein content. The water-soluble albumin was the predominant protein fraction, accounting for 34.5% of

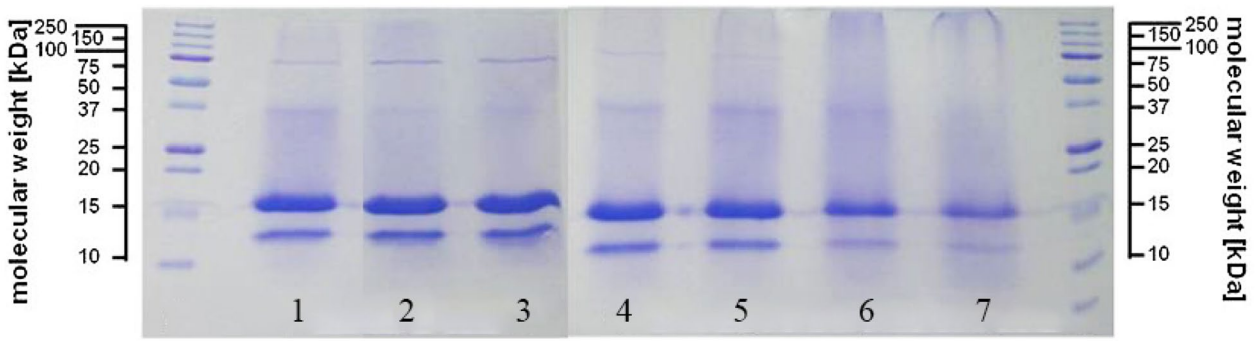

Fig. 8 SDS-PAGE of DWGP:pectin (4:1 w/w and $C_T = 1\%$ w/v). In gel (**A**), lane 1 corresponds to mixtures in start point (0 h); lanes 3–7 correspond to passing of time

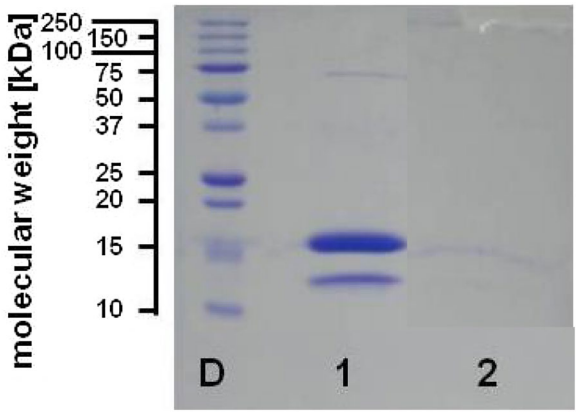

Fig. 9 SDS-PAGE of individually investigated DWGP and pectin samples. Lane 1: DWGP, lane 2: pectin. The pectin sample does not show inherent protein. The lane above letter D contains the protein standard

the total proteins, which was higher than that in wheat flour and rice [66, 67].

To check for the formation of high molecular weight material as an indication of complex coaservation, SDS-PAGE was performed on heat treated DWGP-Pectin mixtures. Reducing conditions were chosen, so that only complex are detected. DWGP-Pectin mixtures are expected to have high molecular weight above 100 kDa [29, 68, 69]. Figure 8 shows SDS-PAGE gel of the DWGP-Pectin mixtures. The lane above the letter corresponds to the protein standard while lanes above numbers contain the investigated samples. Spery-drying of DWGP-Pectin mixtures as one of the step in coaservate preparation did not have any significant influence on the molecular weight of the protein (compare Fig. 1, lanes A1 and 2).

At the beginning, intensely colored bands were visible at 14 kDa, 18 kDa, 37 kDa and 75 kDa, corresponding to monomeric and dimeric, and BSA, respectively (Fig. 8, lanes 1) [29, 70]. No protein containing substances with a molecular weight above 75 kDa were detected at first. Upon passing of time, the characteristic protein bands from DWGP fractions became paler as is described in literature [29, 71, 72].

Substances with a molecular weight above 100 kDa were detected after passing of time (Fig. 8, lanes A4). These substances appeared in the form of polydispersed bands. Due to the polymeric nature of pectin, its molecular weight is not as well defined as that of DWGP. This leads to the formation of complex with a broad molecular weight distribution. After more passing of time (Fig. 8, lanes A7), intensive immobilized bands were seen at the gel injection point. This indicates protein rich substances which were excluded from intrusion into the gel pores because of them being too large in molecular weight and/or volume (> 250 kDa) [73, 75].

SDS-PAGE of separately incubated protein and pectin did not indicate any formation of high molecular weight material (Fig. 9). Therefore, self-polymerization of the single substances did not take place. Only intraction of protein and pectin together led to the formation of high molecular weight species. However, some characheristics of complex coacervate of the wheat germ protein/high methoxy pectin was evaluated here, other properties of the coacervates such as surface activity, molecular structure [76-78], application in drinks and novel algorithms [79-85] needs to be studied in future trends.

Conclusion

The use of wheat germ protein, as a novel plant protein in coacervation with apple high methoxy pectin for encapsulation of D-limonen was investigated. In order to investigate the molecular interactions between DWGP and pectin, turbidimetric analysis, zeta potential, and particle size were measured at different pH levels. Soluble complexes were observed at pH = 6.0 followed by phase separation at $pH_{\phi 1} = 4.9$. The maximum biopolymer interaction was found at pH = 4.0 and CT 1% (w/v). When anionic pectin interacted with cationic protein fragments, complex soluble coacervates were formed between pHc and $pH_{\phi 1}$. Rheological properties were measured. The complexation process was confirmed by physical properties such as FTIR, SEM, and XRD. This study provides valuable information for the design of food ingredients with specific functions based on DWGP and pectin complex. The DWGP-pectin complex cocervate is used in foods for the protection and controlled release of flavors or other sensitive compounds.

Acknowledgements
I would like to express my very great appreciation to Research Institute of Food Sciecne and Technology for its valuable and constructive assistance during the planning and development of this research work.

Author contributions
Hamed Jamshidian: data curation; investigation; methodology; writing-original draft. Ali Rafe: conceptualization; supervision; validation; visualization; writing-review & editing.

Funding
Not applicable.

Availability of data and materials
All data are presented in the manuscript.

Declarations

Ethics approval and consent to participate
The authors will follow the Ethical Responsibilities of Authors and COPE rules. On behalf of all co-authors, I believe the participants are giving informed consent to participate in this study.

Consent for publication
I, HamedJamshidian give my consent for the submitted manuscript to be published in the Chemical and Biological Technologies in Agriculture. II, Ali

Rafe give my consent for the submitted manuscript to be published in the Chemical and Biological Technologies in Agriculture.

Competing interests
The authors declare that they have no competing interests.

Author details
[1]Department of Food Processing, Research Institute of Food Science and Technology (RIFST), PO Box 91735-147, Mashhad, Iran.

Received: 6 January 2024 Accepted: 5 April 2024
Published online: 27 April 2024

References

1. Ghasemi S, Jafari SM, Assadpour E, Khomeiri M. Nanoencapsulation of d-limonene within nanocarriers produced by pectin-whey protein complexes. Food Hydrocoll. 2018;77:152–62.
2. Ge Y, Sun A, Ni Y, Cai T. Study and development of a defatted wheat germ nutritive noodle. Eur Food Res Technol. 2001;212:344–8.
3. Gómez M, González J, Oliete B. Effect of extruded wheat germ on dough rheology and bread quality. Food Bioprocess Technol. 2012;5:2409–18.
4. Moss R. The application of light and scanning electron microscopy during flour milling and wheat processing. Food Struct. 1985;4:16.
5. Li X, Fang Y, Al-Assaf S, Phillips GO, Yao X, Zhang Y, Zhao M, Zhang K, Jiang F. Complexation of bovine serum albumin and sugar beet pectin: structural transitions and phase diagram. Langmuir. 2012;28:10164–76.
6. Ru Q, Wang Y, Lee J, Ding Y, Huang Q. Turbidity and rheological properties of bovine serum albumin/pectin coacervates: effect of salt concentration and initial protein/polysaccharide ratio. Carbohyd Polym. 2012;88:838–46.
7. Fraeye I, Doungla E, Duvetter T, Moldenaers P, Van Loey A, Hendrickx M. Influence of intrinsic and extrinsic factors on rheology of pectin–calcium gels. Food Hydrocoll. 2009;23:2069–77.
8. Salminen H, Weiss J. Electrostatic adsorption and stability of whey protein–pectin complexes on emulsion interfaces. Food Hydrocoll. 2014;35:410–9.
9. Stenger C, Zeeb B, Hinrichs J, Weiss J. Formation of concentrated biopolymer particles composed of oppositely charged WPI and pectin for food applications. J Dispers Sci Technol. 2017;38:1258–65.
10. Zeeb B, Schöck V, Schmid N, Majer L, Herrmann K, Hinrichs J, Weiss J. Impact of food structure on the compatibility of heated WPI–pectin-complexes in meat dispersions. Food Funct. 2018;9:1647–56.
11. Zeeb B, Stenger C, Hinrichs J, Weiss J. Formation of concentrated particles composed of oppositely charged biopolymers for food applications–impact of processing conditions. Food Struct. 2016;10:10–20.
12. Esfanjani AF, Jafari SM, Assadpoor E, Mohammadi A. Nano-encapsulation of saffron extract through double-layered multiple emulsions of pectin and whey protein concentrate. J Food Eng. 2015;165:149–55.
13. Esfanjani AF, Jafari SM, Assadpour E. Preparation of a multiple emulsion based on pectin-whey protein complex for encapsulation of saffron extract nanodroplets. Food Chem. 2017;221:1962–9.
14. Mohammadi A, Jafari SM, Assadpour E, Esfanjani AF. Nano-encapsulation of olive leaf phenolic compounds through WPC–pectin complexes and evaluating their release rate. Int J Biol Macromol. 2016;82:816–22.
15. Mendelsohn J, Barrett CJ, Chan V, Pal A, Mayes A. Rubner, MF, fabrication of microporous thin films from polyelectrolyte multilayers. Langmuir. 2000;16:5017–23.
16. Gharehbeglou P, Jafari SM, Hamishekar H, Homayouni A, Mirzaei H. Pectin-whey protein complexes vs. small molecule surfactants for stabilization of double nano-emulsions as novel bioactive delivery systems. J Food Engin. 2019;245:139–48.
17. Raei M, Shahidi F, Farhoodi M, Jafari SM, Rafe A. Application of whey protein-pectin nano-complex carriers for loading of lactoferrin. Int J Biol Macromol. 2017;105:281–91.
18. Klemmer K, Waldner L, Stone A, Low N, Nickerson M. Complex coacervation of pea protein isolate and alginate polysaccharides. Food Chem. 2012;130:710–5.
19. Aryee FN, Nickerson MT. Formation of electrostatic complexes involving mixtures of lentil protein isolates and gum Arabic polysaccharides. Food Res Int. 2012;48:520–7.
20. Elmer C, Karaca AC, Low NH, Nickerson MT. Complex coacervation in pea protein isolate–chitosan mixtures. Food Res Int. 2011;44:1441–6.
21. Niu F, Su Y, Liu Y, Wang G, Zhang Y, Yang Y. Ovalbumin–gum arabic interactions: effect of pH, temperature, salt, biopolymers ratio and total concentration. Coll Surf B. 2014;113:477–82.
22. Ibáñez MD, Sanchez-Ballester NM, Blázquez MA. Encapsulated limonene: a pleasant lemon-like aroma with promising application in the agri-food industry. Rev Mol. 2020;25:2598.
23. Lan Y, Ohm J-B, Chen B, Rao J. Phase behavior and complex coacervation of concentrated pea protein isolate-beet pectin solution. Food Chem. 2020;307: 125536.
24. AOAC. Official methods of analysis, in, Aoac Washington, DC. AOAC: Rockville; 1990.
25. Hasanvand E, Rafe A, Emadzadeh B. Phase separation behavior of flaxseed gum and rice bran protein complex coacervates. Food Hydrocoll. 2018;82:412–23.
26. Weinbreck F, De Vries R, Schrooyen P, De Kruif C. Complex coacervation of whey proteins and gum arabic. Biomacromol. 2003;4:293–303.
27. Zou W, Mourad FK, Zhang X, Ahn DU, Cai Z, Jin Y. Phase separation behavior and characterization of ovalbumin and propylene glycol alginate complex coacervates. Food Hydrocoll. 2020;108: 105978.
28. Muhoza B, Xia S, Cai J, Zhang X, Duhoranimana E, Su J. Gelatin and pectin complex coacervates as carriers for cinnamaldehyde: effect of pectin esterification degree on coacervate formation, and enhanced thermal stability. Food Hydrocoll. 2019;87:712–22.
29. Schmidt US, Pietsch V, Rentschler C, Kurz T, Endreß H-U, Schuchmann H. Influence of the degree of esterification on the emulsifying performance of conjugates formed between whey protein isolate and citrus pectin. Food Hydrocoll. 2016;56:1–8.
30. Ach D, Briançon S, Dugas V, Pelletier J, Broze G, Chevalier Y. Influence of main whey protein components on the mechanism of complex coacervation with *Acacia* gum. Coll Surf A. 2015;481:367–74.
31. Souza CJ, Garcia-Rojas EE. Interpolymeric complexing between egg white proteins and xanthan gum: effect of salt and protein/polysaccharide ratio. Food Hydrocoll. 2017;66:268–75.
32. Schmitt C, Aberkane L, Sanchez C. Protein–polysaccharide complexes and coacervates. In: Schmitt C, Aberkane L, Sanchez C, editors. Handbook of hydrocolloids. Elsevier: Amsterdam; 2009. p. 420–76.
33. Guzey D, McClements DJ. Formation, stability and properties of multilayer emulsions for application in the food industry. Adv Coll Interfac Sci. 2006;128:227–48.
34. Harnsilawat T, Pongsawatmanit R, McClements D. Characterization of β-lactoglobulin–sodium alginate interactions in aqueous solutions: a calorimetry, light scattering, electrophoretic mobility and solubility study. Food Hydrocoll. 2006;20:577–85.
35. Girard M, Turgeon SL, Gauthier SF. Interbiopolymer complexing between β-lactoglobulin and low-and high-methylated pectin measured by potentiometric titration and ultrafiltration. Food Hydrocoll. 2002;16:585–91.
36. Liu J, Shim YY, Wang Y, Reaney MJ. Intermolecular interaction and complex coacervation between bovine serum albumin and gum from whole flaxseed (*Linum* usitatissimum L.). Food Hydrocoll. 2015;49:95–103.
37. Liu J, Shim YY, Shen J, Wang Y, Reaney MJ. Whey protein isolate and flaxseed (*Linum* usitatissimum L.) gum electrostatic coacervates: turbidity and rheology. Food Hydrocoll. 2017;64:18–27.
38. Warr J, Michaud P, Picton L, Muller G, Courtois B, Ralainirina R, Courtois J. Large-scale purification of water-soluble polysaccharides from flaxseed mucilage, and isolation of a new anionic polymer. Chromatographia. 2003;58:331–5.
39. Gulão EdS, de Souza CJ, da Silva FA, Coimbra JS, Garcia-Rojas EE. Complex coacervates obtained from lactoferrin and gum arabic: formation and characterization. Food Res Int. 2014;65:367–74.
40. Yang Y, Anvari M, Pan C-H, Chung D. Characterisation of interactions between fish gelatin and gum arabic in aqueous solutions. Food Chem. 2012;135:555–61.
41. Ruis HG, Venema P, van der Linden E. Relation between pH-induced stickiness and gelation behaviour of sodium caseinate aggregates as determined by light scattering and rheology. Food Hydrocoll. 2007;21:545–54.
42. Rodsamran P, Sothornvit R. Microwave heating extraction of pectin from lime peel: characterization and properties compared with the conventional heating method. Food Chem. 2019;278:364–72.

43. Dranca F, Vargas M, Oroian M. Physicochemical properties of pectin from Malus domestica 'Fălticeni'apple pomace as affected by non-conventional extraction techniques. Food Hydrocoll. 2020;100: 105383.
44. Lv Y, Yang F, Li X, Zhang X, Abbas S. Formation of heat-resistant nanocapsules of jasmine essential oil via gelatin/gum arabic based complex coacervation. Food Hydrocoll. 2014;35:305–14.
45. Chatterjee S, Salaün F, Campagne C. Development of multilayer microcapsules by a phase coacervation method based on ionic interactions for textile applications. Pharmaceutics. 2014;6:281–97.
46. Gorji SG, Gorji EG, Mohammadifar MA. Characterisation of gum tragacanth (*Astragalus* gossypinus)/sodium caseinate complex coacervation as a function of pH in an aqueous medium. Food Hydrocoll. 2012;30:1e8.
47. Huang G, Xiao J, Wang S, Qiu H. Rheological properties of O-carboxymethyl chitosan–gum Arabic coacervates as a function of coacervation pH. Food Hydrocoll. 2015;43:436–41.
48. Raei M, Rafe A, Shahidi F. Rheological and structural characteristics of whey protein-pectin complex coacervates. J Food Eng. 2018;228:25–31.
49. Mangavel C, Barbot J, Popineau Y, Guéguen J. Evolution of wheat gliadins conformation during film formation: a fourier transform infrared study. J Agric Food Chem. 2001;49:867–72.
50. Kong J, Yu S. Fourier transform infrared spectroscopic analysis of protein secondary structures. Acta Biochim Biophys Sin. 2007;39:549–59.
51. Zhou LinYi ZL, Yang Yong YY, Ren HaiBin RH, Zhao Yan ZY, Wang ZhongJiang WZ, Wu Fei WF, Xiao ZhiGang XZ. Structural changes in rice bran protein upon different extrusion temperatures a Raman spectroscopy study. J Chem. 2016. https://doi.org/10.1155/2016/6898715.
52. Maciel VBV, Yoshida CM, Franco TT. Chitosan/pectin polyelectrolyte complex as a pH indicator. Carbohyd Polym. 2015;132:537–45.
53. Huang G-Q, Sun Y-T, Xiao J-X, Yang J. Complex coacervation of soybean protein isolate and chitosan. Food Chem. 2012;135:534–9.
54. Sun C, Dai L, Gao Y. Formation and characterization of the binary complex between zein and propylene glycol alginate at neutral pH. Food Hydrocoll. 2017;64:36–47.
55. Gilsenan P, Richardson R, Morris E. Associative and segregative interactions between gelatin and low-methoxy pectin: Part 1. associative interactions in the absence of Ca2+. Food Hydrocoll. 2003;17:723–37.
56. Guerrero P, Garrido T, Leceta I, de la Caba K. Films based on proteins and polysaccharides: preparation and physical–chemical characterization. Eur Polymer J. 2013;49:3713–21.
57. Cava D, Catala R, Gavara R, Lagaron JM. Testing limonene diffusion through food contact polyethylene by FT-IR spectroscopy: film thickness, permeant concentration and outer medium effects. Polym Test. 2005;24:483–9.
58. Lan WeiJie LW, Liang Xue LX, Lan WentIng LW, Ahmed S, Liu YaoWen LY, Qin Wen QW. Electrospun polyvinyl alcohol/D-limonene fibers prepared by ultrasonic processing for antibacterial active packaging material. Molecules. 2019. https://doi.org/10.3390/molecules24040767.
59. Lan W, Wang S, Chen M, Sameen DE, Lee K, Liu Y. Developing poly (vinyl alcohol)/chitosan films incorporate with d-limonene: study of structural, antibacterial, and fruit preservation properties. Int J Biol Macromol. 2020;145:722–32.
60. Jain A, Thakur D, Ghoshal G, Katare O, Shivhare U. Characterization of microcapsulated β-carotene formed by complex coacervation using casein and gum tragacanth. Int J Biol Macromol. 2016;87:101–13.
61. Ordoñez M, Herrera A. Morphologic and stability cassava starch matrices for encapsulating limonene by spray drying. Powder Technol. 2014;253:89–97.
62. Yang X, Gao N, Hu L, Li J, Sun Y. Development and evaluation of novel microcapsules containing poppy-seed oil using complex coacervation. J Food Eng. 2015;161:87–93.
63. Kaushik P, Dowling K, McKnight S, Barrow CJ, Adhikari B. Microencapsulation of flaxseed oil in flaxseed protein and flaxseed gum complex coacervates. Food Res Int. 2016;86:1–8.
64. Silva KA, Coelho MAZ, Calado VM, Rocha-Leão MH. Olive oil and lemon salad dressing microencapsulated by freeze-drying, LWT-food. Sci Technol. 2013;50:569–74.
65. Zhu KX, Zhou HM, Qian HF. Proteins extracted from defatted wheat germ: nutritional and structural properties. Cereal Chem. 2006;83:69–75.
66. Padhye V, Salunkhe D. Extraction and characterization of rice proteins. Cereal Chem. 1979;56(5):389–393.
67. Wrigley C, Bietz J. Proteins and amino acids. Wheat Chem Technol. Volume I., 1988, No. Ed. 3, 159–275.
68. Akhtar M, Dickinson E. Whey protein–maltodextrin conjugates as emulsifying agents: an alternative to gum arabic. Food Hydrocoll. 2007;21:607–16.
69. Einhorn-Stoll U, Ulbrich M, Sever S, Kunzek H. Formation of milk protein–pectin conjugates with improved emulsifying properties by controlled dry heating. Food Hydrocoll. 2005;19:329–40.
70. Neirynck N, Van der Meeren P, Gorbe SB, Dierckx S, Dewettinck K. Improved emulsion stabilizing properties of whey protein isolate by conjugation with pectins. Food Hydrocoll. 2004;18:949–57.
71. Al-Hakkak J, Al-Hakkak F. Functional egg white–pectin conjugates prepared by controlled maillard reaction. J Food Eng. 2010;100:152–9.
72. Xu D, Wang X, Jiang J, Yuan F, Gao Y. Impact of whey protein–Beet pectin conjugation on the physicochemical stability of β-carotene emulsions. Food Hydrocoll. 2012;28:258–66.
73. Kasran M, Cui SW, Goff HD. Emulsifying properties of soy whey protein isolate–fenugreek gum conjugates in oil-in-water emulsion model system. Food Hydrocoll. 2013;30:691–7.
74. Bendit E. A quantitative x-ray diffraction study of the alpha-beta transformation in wool keratin. Text Res J. 1960;30:547–55.
75. Neirynck N, Van der Meeren P, Lukaszewicz-Lausecker M, Cocquyt J, Verbeken D, Dewettinck K. Influence of pH and biopolymer ratio on whey protein–pectin interactions in aqueous solutions and in O/W emulsions. Colloids Surf A Physicochem Eng Asp. 2007;298:99–107.
76. Dou J, Liu J, Wang Y, Zhi L, Shen J, Wang G. Surface activity, wetting, and aggregation of a perfluoropolyether quaternary ammonium salt surfactant with a hydroxyethyl group. Molecules. 2023;28(20):7151.
77. Chen B, Zhang X, Liu Y, Ma X, Wang X, Cao X, et al. Magnetic porous carbons derived from iron-based metal-organic framework loaded with glucose for effective extraction of synthetic organic dyes in drinks. J Chromatogr A. 2022;1661:462716. https://doi.org/10.1016/j.chroma.2021.462716
78. Rong F, Yufan G, Junhuai LI, Bo HU, Lu Y. An improved BPNN method based on probability density for indoor location IEICE transactions on information and systems. 2023;E106-D(5):773–85. https://doi.org/10.1587/transinf.2022DLP0073
79. Zheng Y, Wang Y, Liu J. Research on structure optimization and motion characteristics of wearable medical robotics based on Improved Particle Swarm Optimization Algorithm Future Generation Computer Systems. 2022;129:187–98 https://doi.org/10.1016/j.future.2021.11.021
80. Guangming Z, Wenhai L, Miao Y, Hui H, Yaning W, Zhifeng H, et al. Electric-Field-Driven Printed 3D Highly Ordered Microstructure with Cell Feature Size Promotes the Maturation of Engineered Cardiac Tissues. Abstract Advanced Science. 2023;10(11):e2206264. https://doi.org/10.1002/advs.202206264
81. Liao L, Guo Z, Gao Q, Wang Y, Yu F, Zhao Q, et al. Color image recovery using generalized matrix completion over higher-order finite dimensional algebra. Axioms 2023;12(10):954. https://doi.org/10.3390/axioms12100954
82. Jiang L. A fast and accurate circle detection algorithm based on random sampling Future Generation Computer Systems 2021;123:245–56. https://doi.org/10.1016/j.future.2021.05.010
83. Wang J, Xu Z, Zheng X, Liu Z. A fuzzy logic path planning algorithm based on geometric landmarks and kinetic constraints. Inf Technol Contr. 2022;51(3):499–514. https://doi.org/10.5755/j01.itc.51.3.30016
84. Li J, Tang H, Li X, Dou H, Li R. LEF-YOLO: a lightweight method for intelligent detection of four extreme wildfires based on the YOLO framework. Int J Wildland Fire. 2024;33(1). https://doi.org/10.1071/WF23044
85. Chen C, Han D, Shen X. CLVIN: Complete language-vision interaction network for visual question answering Knowledge-Based Systems 2023;275:110706. https://doi.org/10.1016/j.knosys.2023.110706

Publisher's Note